Carbon-Interconnected Ge Nanocrystals as an Anode with Ultra-Long-Term Cyclability for Lithium Ion Batteries

*Duc Tung Ngo, Ramchandra S. Kalubarme, Hang T. T. Le, John G. Fisher, Choong-Nyeon Park, Il-Doo Kim, and Chan-Jin Park**

Germanium (Ge) possesses a great potential as a high-capacity anode material for lithium ion batteries but suffers from its poor capacity retention and rate capability due to significant volume expansion by lithiation. Here, a facile synthetic route is introduced for producing nanometer-sized Ge crystallites interconnected by carbon (GEC) via thermal decomposition of a Ge-citrate complex followed by a calcination process in an inert atmosphere. The GEC electrode shows outstanding electrochemical performance, i.e., an almost 98.8% capacity retention of 1232 mAh g^{-1}, even after 1000 cycles at the rate of C/2. Importantly, a high discharge capacity of 880 mAh g^{-1} is maintained at the very high rate of 10 C. The excellent anode performance of GEC stems from both effective buffering of carbon anchored to the Ge nanocrystals and the high open porosity of the GEC aggregated powder with an average pore diameter of 32 nm. Furthermore, the interfacial layer formed between Ge and carbon plays an essential role in prolonging the cycle life. The GEC electrode can be successfully employed as an anode for next generation lithium ion batteries.

1. Introduction

Among the group IV elements, germanium (Ge) is a potential candidate to replace the conventionally used graphite anodes for lithium ion batteries (LIB). Due to the limitation of the specific capacity of graphite, it cannot meet the worlds' growing demand for batteries with high energy density and high rate capability.[1,2] Although the gravimetric capacity of Ge (1624 mAh g^{-1}) is lower than that of Si (4200 mAh g^{-1}), the volumetric capacity of Ge (7366 Ah l^{-1}) is approximate to that of Si (8344 Ah l^{-1}) due to the higher density of Ge compared to Si.[3–11] Currently, Ge is still more expensive than Si. Nevertheless, Ge is also an abundant element in the earth's crust, and increasing interest and progress in the production technology will most likely lead to a reduction of the price.[11] Furthermore, Ge shows several advantages over silicon: (1) The diffusion coefficient of Li in Ge is approximately two orders of magnitude greater than that in Si.[8,11–13] (2) The intrinsic electrical conductivity of Ge is four orders of magnitude higher than that of Si due to its smaller bandgap.[8,14] (3) The volume expansion during Li insertion into Ge is smaller compared to that of Si.[5,15–17] Thus, the Ge anode can provide a high energy density and ultra-rate capability when coupled with ultra-high rate cathode materials such as $LiFe_{0.9}P_{0.95}O_{4-\delta}$.[18]

Despite these promising characteristics, the capacity fade of the Ge electrode after several charge–discharge cycles is the main problem to be addressed. In order to improve the cyclability of Ge, most previous studies have focused on using a buffer layer and reducing the particle size of Ge.[12,13,15,19–22] The use of a buffer layer has a negligible effect on the specific capacity of Ge. However, it can improve the performance of Ge significantly at high charge-discharge rates owing to improvements of the mechanical properties, contact between the active material and the current collector, and the high diffusivity of lithium. The reduction of the particle size can mitigate the pulverization of the electrode materials. In addition, the small primary particles exhibit a large surface area for charge transfer reactions and reduce the diffusion length of Li^+, thereby improving the cell performance.

Among the various strategies, the use of a carbon buffer layer is the best choice due to the light weight and relatively low cost of carbon. In several previous reports, the use of carbon as a buffer layer has shown promising results; both cyclability and specific capacity have been improved. However, the synthesis process for Ge embedded in a carbon buffer layer is rather complicated and costly. Accordingly, large scale applications based on a Ge anode containing a carbon buffer are rare.[12,13,19,21]

The use of other types of carbon, such as carbon nanotubes and graphene, also can improve the stability and performance of Ge.[15,17,20,23,24] Nevertheless, the use of a large amount of these materials not only reduces the specific capacity of the electrode but also increases the production costs due to the high cost of carbon nanotubes and graphene.

The synthesis of Ge can be classified into two main categories: (1) Chemical vapor deposition (CVD), in which raw materials, such as germane (GeH_4), phenyltrimethylgermane

D. T. Ngo, Dr. R. S. Kalubarme, H. T. T. Le,
Prof. J. G. Fisher, Prof. C.-N. Park, Prof. C.-J. Park
Department of Materials Science and Engineering
Chonnam National University
77, Yongbong-ro, Buk-gu, Gwangju 500–757, South Korea
E-mail: parkcj@jnu.ac.kr
Prof. I.-D. Kim
Department of Materials Science and Engineering
Korea Advanced Institute of Science and Technology (KAIST)
291, Daehak-ro, Yuseong-gu, Daejeon 305–701, South Korea

DOI: 10.1002/adfm.201400888

($C_9H_{14}Ge$), and diphenylgermane ($C_{12}H_{10}Ge$), are used as a source of Ge.[5,13,20,25] However, due to the complicated processing and expensive precursor chemicals, this method is only suitable for the synthesis of small amounts of Ge in the laboratory. (2) Chemical methods for the synthesis of Ge, which involve the use of extremely strong reducing agents, such as sodium borohydride ($NaBH_4$) or oleyamine ($C_{18}H_{37}N$), to reduce $GeCl_4$ and $GeBr_2$ to Ge.[19,21,24] This method can be used to synthesize larger amounts of Ge, but it is harmful to the environment. Safe synthesis of large amounts of Ge with a carbon coating is a considerable challenge.

Therefore, the development of a green, simple, and cost-effective method for the Ge synthesis is necessary. In this study, we introduce a simple method for the synthesis of Ge interconnected by a carbon buffer layer (GEC) using GeO_2 and citric acid. GeO_2 was preferred as the Ge precursor because it is less expensive than other germanium compounds. The Ge nanocrystals interconnected by a carbon buffer layer obtained in this study showed a specific capacity of 1247 mAh g^{-1} with a capacity retention of 98.8% after more than 1000 cycles. When increasing the rate of charge-discharge up to 10 C, the specific capacity only decreased by 30% compared with the specific capacity measured at a C/10 rate. The formation of both Ge nanostructures with particle sizes of ≈50 nm interconnected by carbon and an interfacial layer between Ge and carbon is the key to improve the performance of Ge. Herein, the main problems of capacity fade, poor cyclability, and low coulombic efficiency caused by the pulverization, agglomeration, and loss of contact during the charge-discharge process in Ge-based electrode have been solved.

2. Results and Discussion

In this study, Ge nanoparticles interconnected by a carbon buffer layer were prepared according to the following procedure: citric acid (H_4Cit) and germanate [$Ge(OH)_4^0$] with a molar ratio of 2:1 were mixed to form the complex [$Ge(OH)_2(H_2Cit)_2^{2-}$]. The pH of the complex was adjusted to ≈3.6 by the addition of NH_4OH. Subsequently, the complex was decomposed at 375 °C in air for 3 h to produce amorphous GeO_2 distributed in a carbon matrix and to control the carbon content. Finally, the obtained product was reduced in a continuous flux of argon gas for 3 h at 700, 750, and 850 °C to compare the effect of the reducing temperature on the electrochemical properties of the material. Hereafter, the samples obtained after the decomposition of the Ge-citrate complex will be denoted as follows: the sample prepared at 375 °C in air for 3 h will be denoted as "GeO_2/C" the sample reduced at 700 °C from GeO_2/C as "GEC-700"; the sample reduced at 750 °C from GeO_2/C as "GEC-750"; and the sample reduced at 850 °C from GeO_2/C as "GEC-850." The scheme for the synthesis of GEC is depicted in **Figure 1**.

Figure 2a-d present the X-ray diffraction patterns (XRD) of GeO_2/C, GEC-700, GEC-750, and GEC-850, respectively. The obtained GeO_2/C product (Figure 2a) exhibited a broad diffraction peak with low intensity, indicating that the product obtained at this step has an amorphous structure.

Figure S1a,b (Supporting Information) shows X-ray photoelectron spectroscopy (XPS) spectra for the GeO_2/C product. A peak was observed at the binding energy of 32.25 eV, corresponding to Ge^{4+}. The XRD patterns and XPS spectra confirm that the formed product was amorphous GeO_2 and no peaks corresponding to Ge or its compounds were detected. The two peaks observed at ≈1350 and ≈1560 cm^{-1} in the Raman spectra (Figure S1c, Supporting Information) are characteristics of the disorder-induced D band and graphitic G band of carbon, respectively.[26–28] It can be concluded that the sample contains amorphous GeO_2 and carbon. Themogravimetric analysis (TGA) (Figure S1d, Supporting Information) shows that the GeO_2 content in GeO_2/C was 59.55%. Furthermore, the GEC-700 sample that had been prepared by annealing of GeO_2/C at 700 °C in argon for 3 h did not show any peak related to Ge in the XRD pattern (Figure 2b). The XRD patterns of GeO_2/C and GEC-700 reveal amorphous structures and do not show any distinct feature of crystallinity. The XRD analysis indicates that the reaction between GeO_2 and carbon did not occur at 700 °C. Complete transformation of amorphous GeO_2 to crystalline Ge after the reduction heat treatment is observed for GEC-750

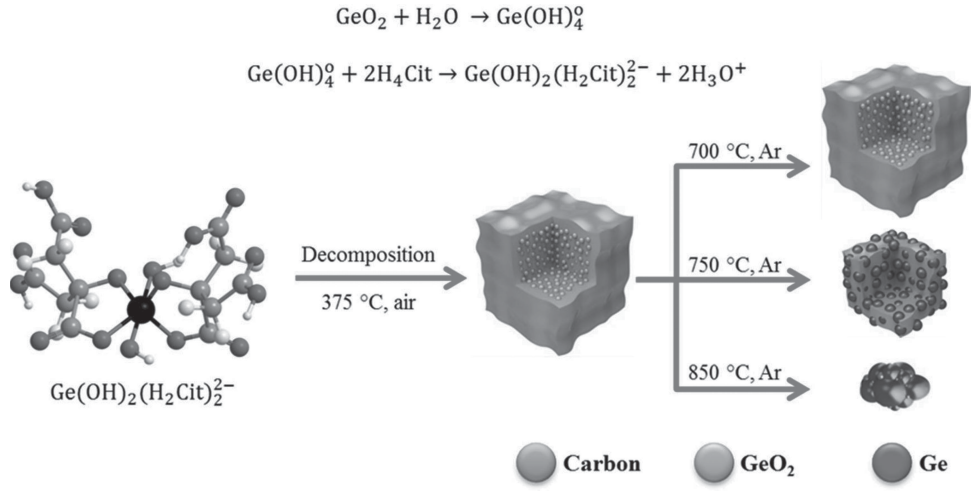

Figure 1. Schematic representation of the two-step synthetic route to GEC.

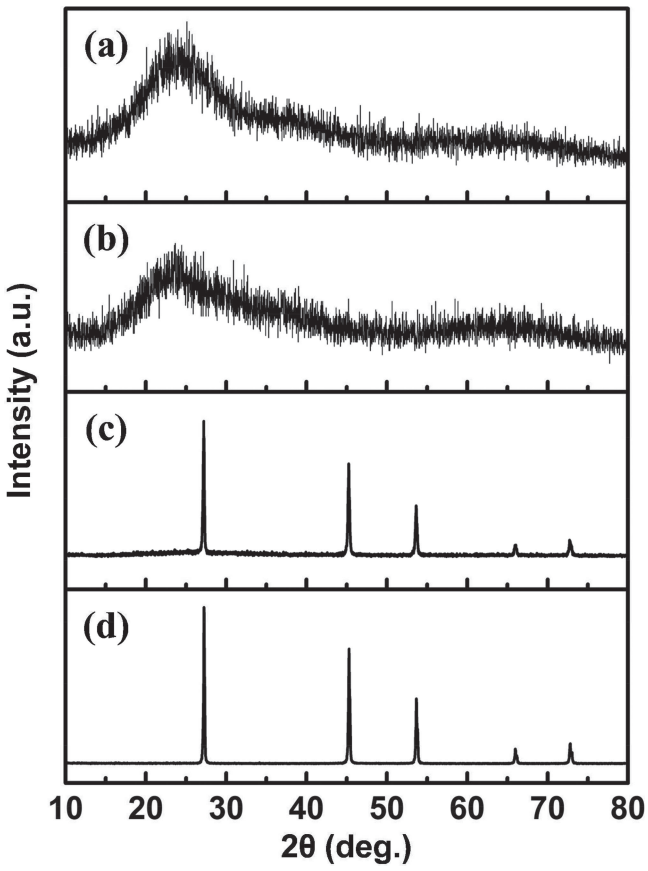

Figure 2. X-ray diffraction patterns (XRD) of a) GeO_2/C, b) GEC-700, c) GEC-750, and d) GEC-850.

and GEC-850, as shown in the XRD patterns in Figure 2c,d. All peaks are consistent with the cubic phase (JCPDS no.65–0333) of Ge, and no additional peaks were observed.

The reaction between GeO_2 and carbon has been described in the literature.[29] According to this report, the reduction of GeO_2 by carbon starts in the temperature range of 827–845 °C, although at this temperature the reaction occurs very slowly. In our study, for amorphous GeO_2 distributed in a carbon matrix, the reduction reaction between GeO_2 and carbon was complete after heating at 750 °C in argon for 3 h. The decrease in reaction temperature observed in the present work compared with the previous report reveals that nanometer-sized amorphous GeO_2 reacts with carbon more easily than crystalline GeO_2, most likely because of the high surface activity of nanometer-sized GeO_2.

The presence of carbon in GEC-750 and GEC-850 was confirmed by Raman spectroscopy as shown in Figure S2 (Supporting Information). Two main peaks were observed at ≈1350 and ≈1560 cm^{-1} corresponding to the disorder-induced D band and the graphitic G band of carbon, respectively. The peak observed at ≈290 cm^{-1} in the Raman spectrum is related to Ge. The relative intensity ratio of the G and D band of GEC-750 and GEC-850 was about 1.06 and 1.04, respectively. From Raman spectroscopy, it can be concluded that GEC-750 and GEC-850 contain amorphous carbon.[26–28]

The morphologies of the samples were investigated using scanning electron microscopy (SEM). **Figure 3** shows SEM images of GEC-750 and GEC-850 powders. For GEC-750, the nanoparticles were connected to each other as shown in Figure 3b. In addition, clusters with a size of 60 μm were formed due to the aggregation of particles (see Figure 3a). For GEC-850, the nanometer-sized particles almost disappeared,

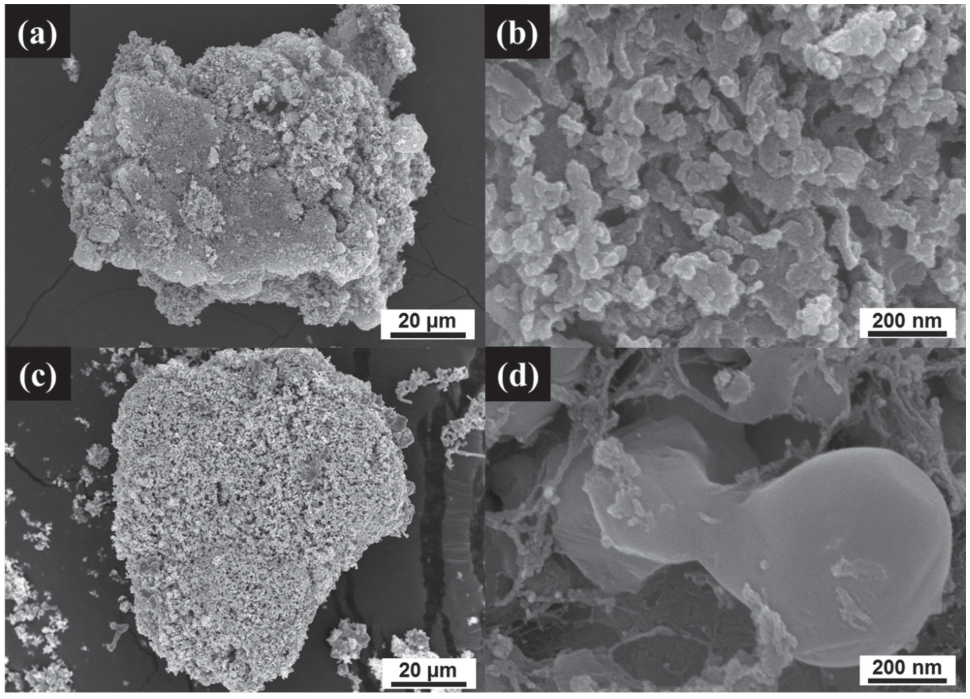

Figure 3. a) Low- and b) high-magnification SEM images of GEC-750; c) low- and d) high-magnification images of GEC-850.

but larger particles with a size of 200–500 nm were observed instead (Figure 3c,d). Larger particles were obtained at higher reduction temperatures. Therefore, loss of carbon at the surface at higher temperatures appears to trigger particle growth. Nevertheless, some small particles were observed due to the presence of carbon on the surface serving as a protective layer. The presence of carbon at the particle surface can prevent the agglomeration of fine particles.

The qualitative composition of GEC-750 and GEC-850 was characterized by energy-dispersive X-ray spectroscopy (EDX) elemental mapping. EDX mapping of the samples revealed typical peaks of Ge and carbon and a very small oxygen peak, as shown in Figure S3 (Supporting Information). The appearance of oxygen can be attributed to the oxidation of Ge to GeO_2 during storage or adsorption of oxygen on the surface. All samples showed uniform distributions of carbon and Ge.

The nanostructures of GEC-750 and GEC-850 were further investigated using transmission electron microscopy (TEM) as shown in **Figure 4**. The TEM images of GEC-750 (Figure 4a,b) reveal that dense areas corresponding to Ge are interconnected by bright grey areas corresponding to carbon. High resolution TEM (HR-TEM) of GEC-750 (Figure 4c) shows that the Ge nanocrystals were embedded in a carbon matrix with a thickness higher than 10 nm. This is in good agreement with scanning transmission electron microscopy (STEM) (Figure 4d) showing a distribution of Ge in carbon. Elemental mapping analysis using energy dispersive X-ray spectroscopy (Figure 4e-f) more directly visualizes Ge (red color) embedded in the carbon matrix (yellow color). The presence of an interconnecting carbon layer is very important for cell performance because it can provide an efficient electric route as reported by Seng et al.[30] The estimated average particle size of Ge was

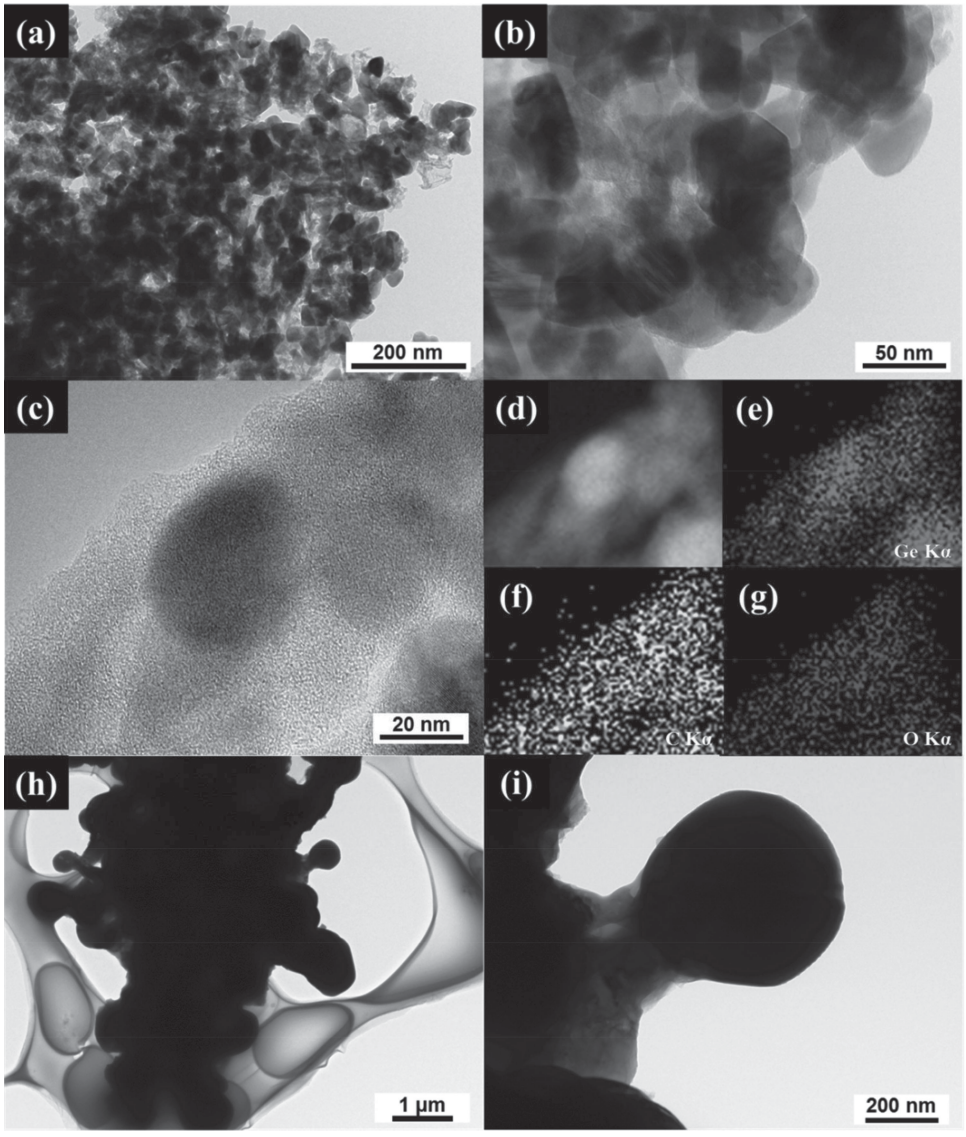

Figure 4. a) Low- and b) high-magnification TEM image of GEC-750, respectively; c) high resolution TEM image of GEC-750; d) STEM image of GEC-750 corresponding to figure (c); TEM-EDX elemental mapping images of e) Ge, f) C and g) O corresponding to figure (c); h) low- and i) high-magnification TEM images of GEC-850, respectively.

Table 1. Elemental composition of GEC-750 and GEC-850.

Sample	Weight Content [wt%]					
	N	C	H	S	O	Ge
GEC-750	0.776	13.139	0.301	0.000	1.101	84.683
GEC-850	0.000	1.422	0.043	0.000	0.136	98.399

The weight contents of nitrogen, carbon, hydrogen, and sulfur are determined by elemental analysis (CHNS-O). The remainder is germanium.

≈50 nm. Moreover, some large dark areas were observed in the TEM images resulting from aggregation of small particles.

The TEM images of GEC-850 (Figure 4h,i) show almost totally dark regions, indicating that the particles are connected with less carbon. Elemental analysis (CHNS-O) confirmed that the carbon content of the GEC-750 and GEC-850 samples was 13.139 and 1.422 wt%, respectively, as shown in **Table 1**.

To determine the surface area, N_2 adsorption/desorption isotherms of the samples were characterized. As shown in Figure S4 (Supporting Information), the GEC-750 sample exhibited a specific area of 40.2 m^2 g^{-1}, an average pore diameter of 32 nm, and a pore volume of 0.321 cm^3 g^{-1}, while the GEC-850 sample exhibited a specific area of 3.2 m^2 g^{-1}, an average pore diameter of 21 nm, and a pore volume of 0.016 cm^3 g^{-1}. The decrease in specific area and pore diameter for GEC-850 compared to GEC-750 is attributed to the increased particle size and loss of carbon.

In order to investigate the electrochemical properties of the samples during the charge-discharge process, the GEC-750 and GEC-850 were assembled into coin-type half-cells. The half-cells were tested within a potential window of 0.01 to 1.5 V vs. Li/Li^+. The cycling performance of the samples is presented in **Figure 5**a. The GEC-750 electrode was tested at C/20 (80 mA g^{-1}) in the first cycle, and a specific capacity of 1302 mAh g^{-1} was

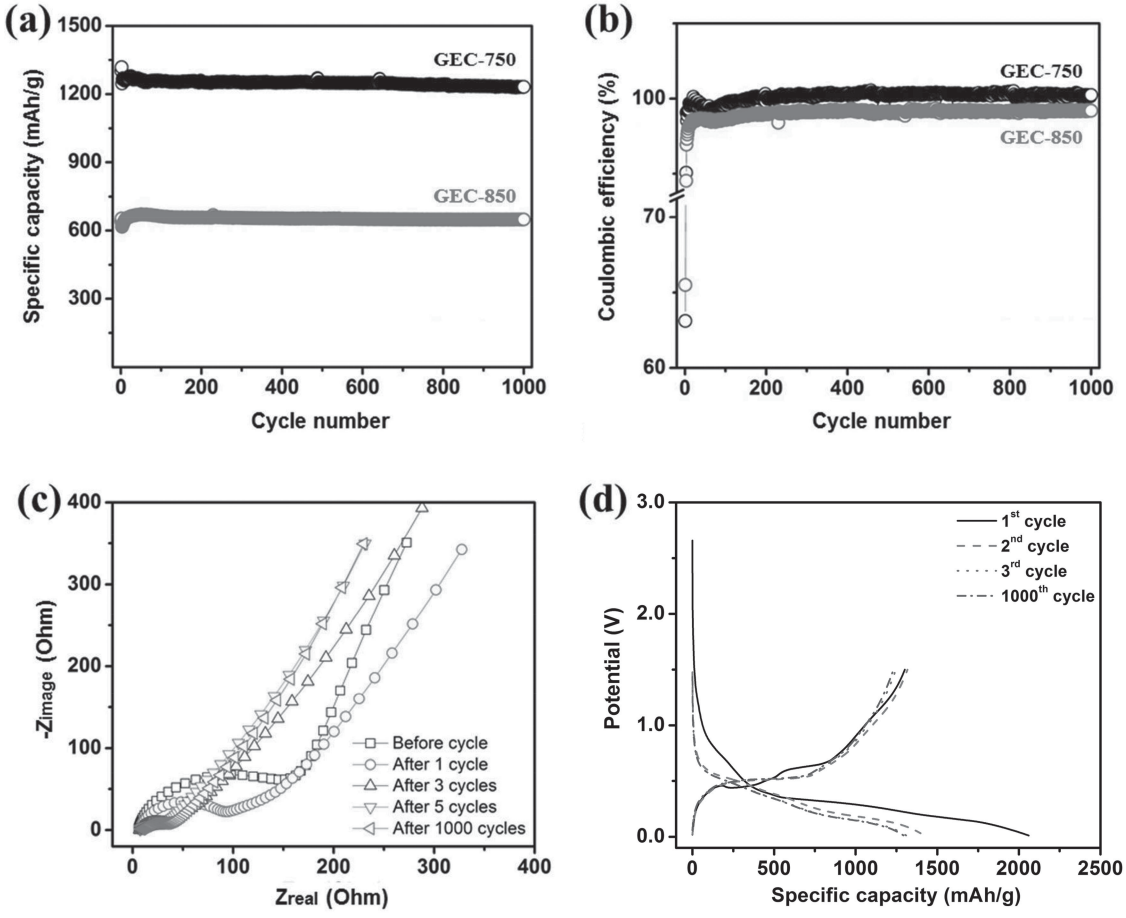

Figure 5. a) Reversible (charge) capacity of GEC-750 and GEC-850 tested at C/20 rate in the first cycle, at C/10 rate in the second cycle, and at C/2 rate in the third and successive cycles; b) coulombic efficiency of GEC-750 and GEC-850; c) electrochemical impedance spectra of GEC-750 after a different number of cycles at full state of charge; d) discharge-charge potential profiles of GEC-750.

measured. Then, the electrode was tested at C/10 (160 mA g^{-1}) in the second cycle, and the obtained specific capacity was 1318 mAh g^{-1}. In the third cycle, the sample was cycled at C/2 (800 mA g^{-1}), and a specific capacity of 1247 mAh g^{-1} was observed. This value is close to the theoretical capacity of Ge (1620 mAh g^{-1}). The high specific capacity of GEC-750 is attributed to the uniform distribution of nanometer-sized Ge particles. As show in Figure 5a, for GEC-850 with a particle size of 200–500 nm, the charge capacity of 617 mAh g^{-1} was observed at the rate of C/2. This value is much lower than that of GEC-750 at the same C-rate. The formation of a Li_xGe alloy barrier layer combined with the large particle size of Ge in GEC-850 prevent the diffusion of lithium ions from the electrolyte to the bulk Ge during the discharge process. In particular, after the formation of the Li_xGe alloy layer, this layer acts as a barrier layer to prevent lithium diffusion, as confirmed in a previous study reporting a low diffusion coefficient of lithium ions in Li_xGe.[31] Thus, this barrier layer causes the core of Ge to become inactive for further lithium alloy formation in the case of GEC-850. On the contrary, due to the larger specific area and pore size and the smaller particle size of GEC-750 compared to those of GEC-850, GEC-750 exhibits more sites for transfer reaction and a shorter diffusion length resulting in a higher specific capacity.[4]

It is noticeable that even after 1000 charge-discharge cycles, the specific capacity of GEC-750 still maintained a high value of 1232 mAh g^{-1}. According to Yoon et al., bare Ge particles of micrometer size are easily broken into 5–15 nm particles during the charge-discharge process, and they exhibit capacity fading when used as an anode for LIB.[12] Accordingly, 5–15 nm is the critical size for size reduction of particles by pulverization during the charge-discharge process. In this study, Ge with a particle size of ≈50 nm interconnected by a carbon buffer layer showed ultra-cyclability during 1000 cycles at C/2 rate. Furthermore, the capacity of the electrode measured after 1000 cycles remained at 98.8% compared to that of the first cycle at the same rate. The ultra-cyclability of GEC-750 is due to the synergy effect of interconnected carbon and pore volume. The interconnected carbon in the sample may work as a buffer layer to moderate the stress, while pores may provide the volume needed for Ge expansion to prevent pulverization. Figure S5 (Supporting Information) displays the morphology of GEC-750 after the 1000th full discharge to 0.1 V vs. Li/Li^+. Even after undergoing 1000 cycles of full charge-discharge under the condition of highest volume expansion of Ge, the morphology of GEC-750 was not changed significantly compared to that of as prepared GEC-750 (Figure 4a,b). This is the reason why even after 1000 cycles the specific capacity of GEC-750 was almost maintained. Herein, the fading capacity of Ge caused by pulverization, agglomeration, and loss of contact during the charge-discharge process is completely solved.[6,15,31] It is demonstrated that porous interconnected carbon is effective in preventing the pulverization and agglomeration of Ge.

Furthermore, to investigate the reversibility of the material, the coulombic efficiency was calculated as shown in Figure 5b. The coulombic efficiency of GEC-750 and GEC-850 in the first cycle was 63.1 and 65.5%, respectively. The coulombic efficiency of GEC-750 in the first cycle was lower than that of GEC-850. This might be due to the higher specific surface area of GEC-750 as compared to GEC-850.[30] After the second cycle, the coulombic efficiency of GEC-750 becomes higher than that of GEC-850, and, after the 20th cycle, the coulombic efficiency of GEC-750 reached a stable value of up to ≈100%. The high coulombic efficiency of GEC-750 is attributed to the carbon-layer covering Ge. A solid electrolyte interphase (SEI) layer can be formed due to the decomposition of the electrolyte on the surface of the electrode at low potential, which contributes to the irreversible capacity. Ge has a very high irreversible capacity compared with carbon.[32,33] This indicates that the decomposition of the electrolyte is easier on the Ge surface than on the carbon surface. By coating Ge with carbon as shown in Figure 4a-c, the direct contact of Ge with the electrolyte can be avoided. Almost all of the SEI is formed on the carbon instead of on the Ge surface, and therefore the irreversible capacity is decreased while the coulombic efficiency can be improved. In order to confirm that the suppressed formation of the SEI layer on the carbon surface presents the main cause of the low irreversible capacity, we investigated the electrochemical impedance of the GEC-750 cell after a different number of cycles. As shown in Figure 5c, before cycling, the charge transfer resistance of the electrode was largest, because the electrode did not undergo any charge/discharge process. After the first cycle, the charge transfer resistance of the electrode significantly decreased due to the surface activation and lattice expansion which triggers lithium ion trasport. After 3 to 5 cycles, the charge transfer resistance became stable. Even after 1000 cycles the electrochemical impedance barely changed, indicating no significant growth of the SEI layer between the fifth cycle and 1000th cycle.

Figure 5d shows the potential profile of GEC-750 during the discharge-charge cycles. The first discharge and charge capacities of GEC-750 at the C/20 rate were 2063 and 1302 mAh g^{-1}, respectively. Interestingly, the first discharge capacity was higher than the theoretical capacity of 1624 mAh g^{-1}. This is due to the formation of a SEI layer on the surface of the material and the native oxide present on the surface of Ge.[5,23,25] The presence of native oxide was confirmed by EDX elemental mapping, as shown in Figure S3 (Supporting Information). For GEC-850, a first discharge capacity of 978 mAh g^{-1} and a charge capacity of 641 mAh g^{-1} were observed, as shown in Figure S6 (Supporting Information).

The rate capability of the GEC-750 electrode was tested at various rates of C/10, C/2, C, 5 C, and 10 C for each of the 10 cycles. The obtained results are shown in **Figure 6**a. The reversible capacity of GEC-750 was 1272, 1229, 1181, 1034, and 881 mAh g^{-1} at rates of C/10, C/2, 1 C , 5 C, and 10 C, respectively. Subsequently, the C-rate was brought back to an initial value of C/10 at which the specific capacity reached a value of 1253 mAh g^{-1} and therefore almost recovered. This value is close to the capacity of the first 10 cycles at this rate. After undergoing an extremely high charge-discharge rate, the capacity rapidly returned to the initial value, indicating the excellent rate capability of the sample. Furthermore, the specific capacity decreased only by about 30% when the rate of charge-discharge increased 100 times. A slight decrease in capacity with increasing the rate of charge-discharge is realized due to the distribution of the carbon buffer layer. Obviously, carbon acts as a channel for lithium to Ge during the insertion/

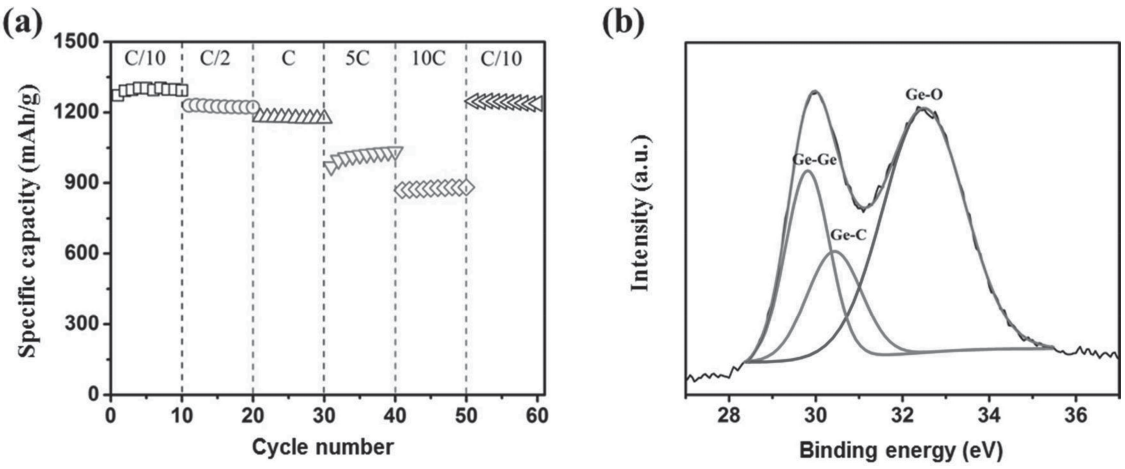

Figure 6. a) Rate capability of GEC-750 at C/10, C/2, 1 C, 5 C, and 10 C; b) high-resolution XPS core spectrum of Ge for the 3d level of GEC-750.

desertion process due to the high diffusion coefficient of carbon compared with germanium.[31,34] Thus, in the presence of carbon, the lithium diffusion can be faster, and the rate capability can be improved. In addition, the carbon buffer layer improves the conductivity of the electrode, thereby improving the performance of the cell at high rate. [35]

Figure 6b shows XPS spectra of the Ge 3d core level obtained from the GEC-750 sample. In Figure 6b, the Ge 3d peak was separated into 3 peaks: Ge-Ge, Ge-C, and Ge-O. The peak corresponding to Ge-Ge was detected at 29.8 eV. This peak demonstrates the formation of Ge during the reaction between GeO_2 and carbon. The binding peaks corresponding to Ge-C and Ge-O were detected at 30.4 and 32.5 eV, respectively.[34,36] The formation of an interfacial layer between Ge-C is due to carbon atoms entering the Ge network. These carbon atoms randomly bond with Ge in sp^3 hybridization to form the interfacial layer.[37] Herein, the interface layer can work as an intermediate elastic layer to accommodate the volume expansion. Thus, the presence of the intermediate elastic layer is believed to be effective in preventing the pulverization of Ge. After 1000 cycles, no fracture or separation of Ge and carbon was observed in the TEM images (Figure S5, Supporting Information).

3. Conclusions

A facile method has been proposed to synthesize nanostructured Ge interconnected by carbon (GEC), based on the simple reduction reaction between amorphous GeO_2 and carbon. The decrease in reaction temperature compared to conventional protocols results from the high surface activity of nanometer-sized GeO_2. GEC-750 exhibits a high specific capacity, superior cyclability, and excellent rate capability as an anode material for LIB. The excellent performance of the sample is due to the nanostructuring of Ge and the presence of a carbon buffer layer, which works as a channel for the supply of lithium during the charge-discharge process. In addition, the formation of an interfacial layer between Ge and C is believed to improve the performance of the material.

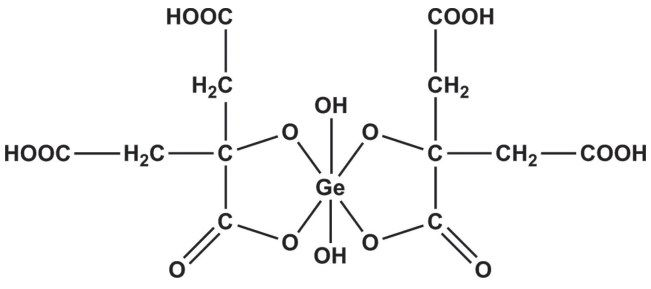

Figure 7. Chemical structure of the Ge-citrate complex.

4. Experimental Section

Material Synthesis: In this study, Ge interconnected by a carbon buffer layer was prepared as follows: Citric acid (H_4Cit) (1 M, 10 ml) and germinate $Ge(OH)_4^0$ (0.5 M, 10 ml) with a molar ratio of 2:1 were mixed to form a complex, and then adjusted to pH = 3.6, by using NH_4OH as previously suggested by Bleb S. Pokrovski et al.[38] They reported that the most stable complex of Ge and citric acid is formed at pH = 3.6. At this pH value, all the germinate forms a complex with citric acid as described in reactions 1 and 2.

$$GeO_2 + 2H_2O \rightarrow Ge(OH)_4^0 \quad (1)$$

$$Ge(OH)_4^0 + 2H_4Cit \rightarrow Ge(OH)_2(H_2Cit)_2^{2-} + 2H_3O^+ \quad (2)$$

The structure of the complex between Ge and citric acid according to Bleb S. Pokrovski et al. is presented in **Figure 7**. Then, the complex was decomposed at 375 °C in air for 3 h to control the carbon content. Finally, the obtained product was reduced in a continuous flux of argon gas for 3 h at 700, 750, and 850 °C to compare the effect of the reducing temperature on the electrochemical properties of the material.

Physical Characterization: GEC-750 and GEC-850 were characterized by high resolution XRD (D/MAX Ultima III, Rigaku, Japan), XPS (Multilab 2000, VG, UK), TGA (TGA-50, Shimadzu, Japan), field emission SEM/EDX (S-4700/EX-200, Hitachi, Japan), HR-TEM (Tecnai G2, Philips, the Netherlands), and Brunauer–Emmett–Teller (BET) analysis (ASAP 2020, Micromeritics, USA).

Electrochemical Characterization: The synthesized powders were mixed with carbon-black and lithium polyacrylate (L-PAA) at a weight ratio of 8:1:1, respectively. Deionized water was added to form a homogeneous

slurry. Then, the slurry was casted onto a copper foil, and the foil was punched into 14 mm diameter disks. Using a casted disk electrode, coin cells (2032 type) were assembled in an argon-filled glove box, with Li metal as the counter electrode and a glass fiber filter (Whatman) soaked with 1 M $LiPF_6$ in ethylene carbonate (EC), dimethyl carbonate (DMC) (1:1, by volume), and 3 wt% fluoride ethylene carbonate (FEC) as the separator. The loading amounts of active materials for all electrodes were about 0.50–0.70 mg. The test electrodes were charged and discharged from 0.01 to 1.5 V vs. Li/Li^+ using an automatic battery cycler (WonATech-WBCS 3000) in order to determine the electrochemical properties. In addition, the electrochemical impedance of cells was measured using Gamry-PC750 at the frequency range from 10 mHz to 100 kHz.

Supporting Information

Supporting Information is available from the Wiley Online Library or from the author.

Acknowledgments

This work was supported by the MOE, Korea, under the National Research Foundation of Korea (NRF) grant (No. 2012R1A2005977) and by the MSIP, Korea, under the Convergence Information Technology Research Center (C-ITRC) support program (NIPA-2013-H0301-13-1009) supervised by the National IT Industry Promotion Agency (NIPA). This work was also supported by the MOTIE, Korea, under Energy Efficiency & Resources Core Technology Program of the Korea Institute of Energy Technology Evaluation and Planning (KETEP) (No. 20112020100110/KIER B4-2462).

Received: March 19, 2014
Published online: June 24, 2014

[1] M. Armand, J. M. Tarascon, *Nature* **2008**, *451*, 652.
[2] J. M. Tarascon, M. Armand, *Nature* **2001**, *414*, 359.
[3] T. Song, H. Cheng, K. Town, H. Park, R. W. Black, S. Lee, W. I. Park, Y. Huang, J. A. Rogers, L. F. Nazar, U. Paik, *Adv. Funct. Mater.* **2014**, *24*, 1458.
[4] A. Magasinski, P. Dixon, B. Hertzberg, A. Kvit, J. Ayala, G. Yushin, *Nat. Mater.* **2010**, *9*, 353.
[5] C. K. Chan, X. F. Zhang, Y. Cui, *Nano Lett.* **2007**, *8*, 307.
[6] J. K. Feng, M. O. Lai, L. Lu, *Electrochim. Acta* **2012**, *62*, 103.
[7] X. H. Liu, S. Huang, S. T. Picraux, J. Li, T. Zhu, J. Y. Huang, *Nano Lett.* **2011**, *11*, 3991.
[8] K. C. Klavetter, S. M. Wood, Y.-M. Lin, J. L. Snider, N. C. Davy, A. M. Chockla, D. K. Romanovicz, B. A. Korgel, J.-W. Lee, A. Heller, C. B. Mullins, *J. Power Sources* **2013**, *238*, 123.
[9] X. Chen, K. Gerasopoulos, J. Guo, A. Brown, C. Wang, R. Ghodssi, J. N. Culver, *ACS Nano* **2010**, *4*, 5366.
[10] M. Gu, Y. Li, X. Li, S. Hu, X. Zhang, W. Xu, S. Thevuthasan, D. R. Baer, J.-G. Zhang, J. Liu, C. Wang, *ACS Nano* **2012**, *6*, 8439.
[11] J. Graetz, C. C. Ahn, R. Yazami, B. Fultz, *J. Electrochem. Soc.* **2004**, *151*, A698.
[12] S. Yoon, C.-M. Park, H.-J. Sohn, *Electrochem. Solid-State Lett.* **2008**, *11*, A42.
[13] S.-H. Woo, S. J. Choi, J.-H. Park, W.-S. Yoon, S. W. Hwang, D. Whang, *J. Electrochem. Soc.* **2013**, *160*, A112.
[14] F.-W. Yuan, H.-J. Yang, H.-Y. Tuan, *ACS Nano* **2012**, *6*, 9932.
[15] J. Cheng, J. Du, *CrystEngComm* **2012**, *14*, 397.
[16] S. C. Jung, J. W. Choi, Y.-K. Han, *Nano Lett.* **2012**, *12*, 5342.
[17] A. M. Chockla, M. G. Panthani, V. C. Holmberg, C. M. Hessel, D. K. Reid, T. D. Bogart, J. T. Harris, C. B. Mullins, B. A. Korgel, *J. Phys. Chem. C* **2012**, *116*, 11917.
[18] B. Kang, G. Ceder, *Nature* **2009**, *458*, 190.
[19] H. Lee, H. Kim, S.-G. Doo, J. Cho, *J. Electrochem. Soc.* **2007**, *154*, A343.
[20] R. A. DiLeo, S. Frisco, M. J. Ganter, R. E. Rogers, R. P. Raffaelle, B. J. Landi, *J. Phys. Chem. C* **2011**, *115*, 22609.
[21] H. Lee, M. G. Kim, C. H. Choi, Y.-K. Sun, C. S. Yoon, J. Cho, *J. Phys. Chem. B* **2005**, *109*, 20719.
[22] X.-L. Wang, W.-Q. Han, H. Chen, J. Bai, T. A. Tyson, X.-Q. Yu, X.-J. Wang, X.-Q. Yang, *J. Am. Chem. Soc.* **2011**, *133*, 20692.
[23] R. A. DiLeo, M. J. Ganter, M. N. Thone, M. W. Forney, J. W. Staub, R. E. Rogers, B. J. Landi, *Nano Energy* **2013**, *2*, 268.
[24] D.-J. Xue, S. Xin, Y. Yan, K.-C. Jiang, Y.-X. Yin, Y.-G. Guo, L.-J. Wan, *J. Am. Chem. Soc.* **2012**, *134*, 2512.
[25] L. P. Tan, Z. Lu, H. T. Tan, J. Zhu, X. Rui, Q. Yan, H. H. Hng, *J. Power Sources* **2012**, *206*, 253.
[26] X. Zhou, Y.-G. Guo, *ChemElectroChem* **2014**, *1*, 83.
[27] K. Naoi, N. Ogihara, Y. Igarashi, A. Kamakura, Y. Kusachi, K. Utsugi, *J. Electrochem. Soc.* **2005**, *152*, A1047.
[28] A. C. Ferrari, J. Robertson, *Phys. Rev. B* **1999**, *61*, 14095.
[29] *Inorganic Reactions and Methods: The Formation of Bonds to C, Si, Ge, Sn, Pb* (Eds: J. J. Zuckerman, A. P. Hagen), Wiley-VCH, Weinheim, Germany **2009**.
[30] K. H. Seng, M.-h. Park, Z. P. Guo, H. K. Liu, J. Cho, *Nano Lett.* **2013**, *13*, 1230.
[31] B. Laforge, L. Levan-Jodin, R. Salot, A. Billard, *J. Electrochem. Soc.* **2008**, *155*, A181.
[32] Y.-S. Han, J.-H. Jung, J.-Y. Leec, *J. Electrochem. Soc.* **2004**, *151*, A291.
[33] C.-M. Hwang, J.-W. Park, *Thin Solid Films* **2010**, *518*, 6590.
[34] K. Persson, V. A. Sethuraman, L. J. Hardwick, Y. Hinuma, Y. S. Meng, A. van der Ven, V. Srinivasan, R. Kostecki, G. Ceder, *J. Phys. Chem. Lett.* **2010**, *1*, 1176.
[35] S. Iwamura, H. Nishihara, T. Kyotani, *J. Power Sources* **2013**, *222*, 400.
[36] J. Vilcarromero, F. C. Marques, *Appl. Phys. A* **2000**, *70*, 581.
[37] M. P. Hernández, M. H. Farías, F. F. Castillón, J. A. Díaz, M. Avalos, L. Ulloa, J. A. Gallegos, H. Yee-Madeiros, *Appl. Surf. Sci.* **2011**, *257*, 5007.
[38] G. S. Pokrovski, J. Schott, *Geochim. Cosmochim. Acta* **1998**, *62*, 3413.